The ISME Journal (2017) 11, 727–740

www.nature.com/ismej

ORIGINAL ARTICLE

Coupled molecular and isotopic evidence for denitrifier controls over terrestrial nitrogen availability

Erin FE Lennon and Benjamin Z Houlton
Department of Land Air and Water Resources, University of California at Davis, Davis, CA, USA

Denitrification removes ecologically available nitrogen (N) from the biosphere and influences both the pace and magnitude of global climate change. Disagreements exist over the degree to which this microbial process influences N-availability patterns across Earth's ecosystems. We combine natural stable isotope methods with qPCR to investigate how denitrifier gene abundance is related to variations in nitrate (NO_3^-) pool sizes across diverse terrestrial biomes and conditions. We analyze NO_3^- isotope composition ($^{15}N/^{14}N$, $^{18}O/^{16}O$) and denitrifier gene *nirS* in 52 soil samples from different California ecosystems, spanning desert, chaparral, oak-woodland/savanna and forest. $\delta^{15}N\text{-}NO_3^-$ correlates positively with $\delta^{18}O\text{-}NO_3^-$ ($P \leqslant 0.03$) and *nirS* abundance ($P = 0.00002$) across sites, revealing the widespread importance of isotopic discrimination by soil denitrifiers. Furthermore, NO_3^- concentrations correlate negatively to *nirS* ($P = 0.002$) and $\delta^{15}N\text{-}NO_3^-$ ($P = 0.003$) across sites. We also observe these spatial relationships in short-term (7-day), *in situ* soil-incubation experiments; NO_3^--depletion strongly corresponds with increased *nirS*, *nirS*/16 rRNA, and enrichment of heavy NO_3^- isotopes over time. Overall, these findings suggest that microbial denitrification can consume plant-available NO_3^- to low levels at multiple time scales, contributing to N-limitation patterns across sites, particularly in moist, carbon-rich soils. Furthermore, our study provides a new approach for understanding the relationships between microbial gene abundance and terrestrial ecosystem functioning.
The ISME Journal (2017) **11,** 727–740; doi:10.1038/ismej.2016.147; published online 9 December 2016

Introduction

Microbial denitrification converts inorganic N ($NO_3^- \rightarrow NO_2^-$) to gaseous N forms ($NO \rightarrow N_2O \rightarrow N_2$), accounting for 26-40% of N outputs from natural terrestrial ecosystems worldwide (Houlton and Bai, 2009; Ciais *et al.*, 2013). Such gaseous N losses directly modulate Earth's climate system via the production of the potent greenhouse gas N_2O, and, in N-limited ecosystems, denitrification has potential to restrict the availability of this nutrient for vegetation CO_2 uptake and carbon (C) sequestration. Denitrification is arguably the most poorly understood process in the terrestrial N cycle, posing a fundamental challenge to the fields of ecosystem- and microbial- ecology alike (Williams *et al.*, 1992; Beckman and Koppenol, 1996; Davidson and Seitzinger, 2006).

Two basic problems have limited our understanding of terrestrial denitrification. The first is systemic to ecology if not all of science—quantifying the relationship between pattern and scale (Levin, 1992). Soil microbial processes are highly dynamic and variable in space and time; yet they control many different aspects of local ecological process and global biogeochemical cycles (Falkowski *et al.*, 2008). In the case of denitrification, microbial ecologists and biogeochemists have pointed to variations in moisture, C and N availability controlling soil denitrification rates within and among global ecosystems (Bai *et al.*, 2012; Groffman, 2012). The second challenge centers on the composition of the air: N_2 is the dominant product of terrestrial denitrifiers, but there are challenges with measuring N_2 from natural terrestrial denitrification directly. The Earth's atmosphere is ~78% N_2 by volume, thus posing a fundamental 'signal to noise' barrier to measuring denitrification fluxes in the field. Studies using ^{15}N tracers offer short-term snapshots of denitrification by tracking ^{15}N-enriched NO_3^- into $^{15}N_2$ and $^{15}N_2O$; however, this approach is limited in naturally low N environments and is highly sensitive to the O_2 levels used during course of incubation experiments (Kulkarni *et al.*, 2014). Extrapolating results from local soil experiments to entire ecosystems thereby represents a perennial challenge in terrestrial denitrification research (Davidson and Seitzinger, 2006).

Correspondence: EFE Lennon, Department of Land Air and Water Resources, University of California, 1 Shields Avenue, Davis, CA 95616, USA.
E-mail: efelennon@gmail.com
Received 11 April 2016; revised 9 September 2016; accepted 16 September 2016; published online 9 December 2016

Here, we combine measures of natural N and oxygen (O) stable isotope composition—which can reflect broader integrated patterns in ecosystem N-cycling (Robinson, 2001)—with quantitative real-time qPCR to advance our understanding of terrestrial denitrification from gene to ecosystem scales (Figure 1). As modern genetic tools have become mainstream, researchers have begun to explore the relationships between microbial community structure and ecosystem functioning (for example, Torsvik and Øvreås, 2002; Frey *et al.*, 2004). Microbial diversity has been measured alongside such important steps in the N cycle as mineralization and nitrification, providing novel insights to the biogeochemical dynamics of ecosystems (Bardgett *et al.*, 1999; Calderon *et al.*, 2001; Jackson *et al.*, 2003). Denitrification studies have similarly identified many microorganisms and enzymes involved in NO_3^- reduction (Knowles, 1982; Hochstein *et al.*, 1988; Zumft, 1997). The *nir* (Nitrite Reductase encoding) genes are of particular interest, because they mark the crucial first gas-formation step in the process (Hochstein *et al.*, 1988)—the point at which denitrification becomes a gaseous N loss from terrestrial environments.

We use qPCR techniques to quantify the relative abundance of nitrite reductase-encoding genes *nirS* and *nirK* (Hochstein *et al.*, 1988; Zumft, 1997). These genes are functionally equivalent but structurally different—*nirS* encoding for heme (cytochrome cd1)-containing enzyme NirS and *nirK* encoding for copper-containing enzyme NirK or Cu-NIR (Hochstein *et al.*, 1988; Zumft, 1997). Generally, denitrifiers possess either *nirS* or *nirK* rather than both (Heylen *et al.*, 2006); a recent study found 10 rare organisms that contradicted this general observation, although the authors did not examine whether both genes were functionally active (Graf *et al.*, 2014). We focus primarily on *nirS* given its widespread abundance across soil types, as supported by previous field and cultured strain studies (Braker *et al.*, 1998; Throback *et al.*, 2004). Furthermore, PCR primers for *nirS* capture most of the known diversity of organisms possessing the gene, whereas, due to *nirK* sequence divergence and taxonomic diversity, PCR primer coverage for *nirK* is more limited (Helen *et al.*, 2016). *Nir* genes have been linked to denitrification rates in soil incubation experiments across different environmental conditions (Smith and Tiedje, 1979; Patra *et al.*, 2005; Attard *et al.*, 2011). However, whether an organism possesses such genes does not necessarily indicate whether they will be expressed and active at a given point in time, with little field-based inquiry into denitrifier gene-abundance vs function relationships.

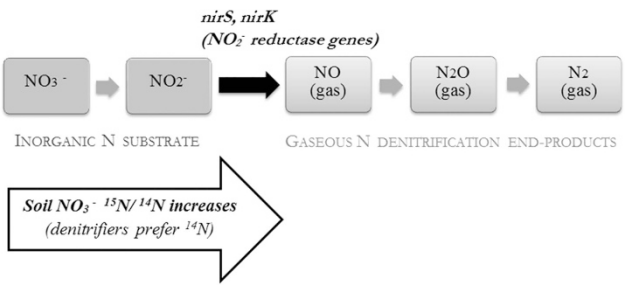

Figure 1 Detecting terrestrial denitrification (Concept). Microbial genes (small scale) can be considered alongside natural stable isotopic signature patterns in soil (large scale) for denitrification at the nitrite (NO_2^-) reduction step. This first gas-formation step marks the point at which denitrification becomes a terrestrial N output.

Natural stable isotope composition offers a complementary, non-disruptive and integrative tool for investigating soil-denitrification across different spatial and temporal scales (Robinson, 2001). Denitrifiers preferentially consume the lighter, more abundant ^{14}N (99.7% of all N) isotope at the expense of the heavier isotope ^{15}N (0.3% of all N), thereby enriching the $^{15}N/^{14}N$ of NO_3^- substrates vs gaseous N products (Mariotti *et al.*, 1981). Over time, such isotopic discrimination ('fractionation') elevates the $^{15}N/^{14}N$ of soil nitrate pools relative to the air (Houlton *et al.*, 2006), and ultimately, ecosystem to global-scale isotopic patterns in the terrestrial biosphere (Houlton and Bai, 2009; Mnich and Houlton, 2015). Other microbial processes could affect isotope signatures in field: nitrification has the potential to lower the $^{15}N/^{14}N$ of NO_3^-; and heterotrophic NO_3^- consumption and other microbial processes (for example, in Dissimilatory Nitrate Reduction to Ammonium (DNRA)) could elevate the $^{15}N/^{14}N$ of NO_3^- substrates similar to denitrification (Fang *et al.*, 2015). Denitrifiers have been shown to increase the $\delta^{15}N$ and $\delta^{18}O$ of NO_3^- within a small range of characteristic slopes (Lehmann *et al.*, 2003; Houlton *et al.*, 2006; Granger *et al.*, 2008), allowing for dual-isotopic evaluation of denitrification's effect on ecosystem NO_3^- availability (Fang *et al.*, 2015). Natural stable isotope budgets have implied utility of forecasting the effect of the terrestrial N cycle on global climate change (Houlton *et al.*, 2015; Zhu and Riley, 2015); however, the importance of microbial-scale denitrification in driving larger $^{15}N/^{14}N$ patterns in ecosystems remains unclear. A particularly open question involves the extent to which denitrification expresses itself on N pools, given the potential for microsite consumption to eliminate the intrinsic isotope effect of denitrifiers on NO_3^- isotopes from local to ecosystem scales (for example, Houlton *et al.*, 2006).

In this study, we ask whether the abundances of soil denitrifier genes are linked to natural stable isotope variations, and we ask whether these cross-scale data can clarify the role of microbial denitrification in regulating patterns of terrestrial NO_3^- availability. Specifically, we combine qPCR-derived *nirS* gene abundances with N and O isotopes of NO_3^- to investigate soil denitrification across redwood forest, oak woodland, chaparral and desert biomes. We complement these field observations with a series of *in-situ* incubation experiments, further

isolating the temporal mechanisms behind the cross-system relationships examined. We use these approaches to test two overarching hypotheses.

The first hypothesis is that there is a significant positive correlation between *nirS* abundance and microbial consumption of lighter N and O isotopes. If supported, this hypothesis would point to a significant link between microbial denitrification at molecular scales and patterns of ecosystem isotopic pools at larger ones. In the absence of such a significant correlation, we would infer that there is no measurable relationship between the abundance of denitrifying genes and isotopic expression. This alternative would point to other processes driving natural isotope abundance patterns.

The second hypothesis is that there is a significant negative correlation among *nirS*/nitrate isotope composition patterns and soil NO_3^- concentrations. This finding would imply that denitrification plays an active role in controlling patterns of NO_3^- availability across ecosystems. However, if denitrification microbial gene abundances and isotopes increase only when NO_3^- is abundant, then we would infer the opposite—that denitrification increases in concert with NO_3^- abundance. If the gene abundances and isotopes do not correlate with NO_3^- levels, we would infer no directional effect either way.

Materials and methods

Study sites

We examined our overarching hypothesis and set of inferences across a matrix of terrestrial sites that occur over a short geographic domain in California (Table 1). Our diverse biome sites range only slightly in latitude (39° 22' N to 34° 47' N) yet represent substantial changes in water availability (Mean Annual Precipitation, MAP, ranged from 1103 to 292 mm across sites) and temperature (−3.9 to 12.0 °C minimum, 33.0–37.8 °C maximum) (Table 1).

Sites fell under a mesic to dry Mediterranean climate, characterized by cool, moist winters and warm, dry summers. Two coastal redwood sites were identified at the Caspar Creek Watershed in Jackson Demonstration State Forest, located near Fort Bragg, California. Four oak woodland and two chaparral sites were selected within the Coast Range of the Mayacamas Mountain foothills, in the University of California's Research and Extension Center. These sites have been exposed to various watershed-scale treatments, including clearcutting (1989 in one redwood site), burning (2003 in two of the oak woodland and 2004 in one of the chaparral sites), prescribed grazing (oak woodland), combinations of burning and grazing (oak woodland), and no disturbance (redwood, oak woodland, chaparral). Total dissolved nitrogen inputs from rainfall and dry deposition at these sites during the time of sampling did not differ significantly, although NO_3^- deposition was slightly higher in oak woodland and chaparral, dissolved organic N deposition more dominant in the redwood sites (Mnich and Houlton, 2015). The oak woodland and chaparral grazed sites may also receive NO_3^- inputs from grazer wastes; also, these sites are closer to farmland than the redwood sites and might receive NO_3^- inputs from fertilizers.

The desert site was located in the Sweeney Granite Mountain Desert Research and Extension Center in the Mojave National Preserve. Owing to patch-scale heterogeneity of the desert site, we divided our sampling scheme into two different categories: 'under shrub/creosote' samples were collected directly under the canopy of the dominant creosote bush, *Larrea tridentata*, and 'interstitial' samples were unvegetated. Any NO_3^- inputs would have to be wind-blown dry deposition, or else fixed from the atmosphere by soil microorganisms, as there was little rainfall at this site.

Field sampling approach

Surface soils (0–15 cm depth, at least five replicates per site) were sampled at all sites over a range of wet (winter) and dry (summer) seasons. This approach allowed us to examine denitrification in the organic soils where C and N concentrations were highest and heterotrophic and rhizosphere activity is most concentrated (Lennon, 2015). For homogenization, soil was sieved to the fine-earth fraction (<2 mm), and roots/organic debris were removed with tweezers. To minimize DNA or isotope cross-contamination, rubber gloves were worn and sampling tools (that is, shovels and trowels) were cleaned with ethanol between collections. Homogenized, fine-fraction, field-moist samples were mixed in half-gallon, resealable polyethylene bags, and subsamples were kept in 60 ml Falcon tubes and immediately put on ice in the field.

Week-long incubation experiments were conducted *in-situ* at redwood ($n=10$), chaparral ($n=10$), desert under-shrub ($n=8$) and desert interstitial ($n=8$) sites to isolate soils from leaching and plant uptake effects. At least 100 g surface soil (0–10 cm depth) was homogenized—using the methods described above—and brought to field capacity with high purity 14.6 M-ohm/cm water in half-gallon, resealable polyethylene bags. Prior to sealing the bags, subsamples were collected in 60 ml Falcon tubes and immediately placed on ice for analyses of initial nutrient, isotope and genetic conditions. The bags were then pressed to expel air, sealed to promote an anaerobic environment and buried in place. Field-incubated samples were collected after 7 days and analyzed for chemistry, isotopes and *nir* abundance.

Soil moisture

Pre-weighed tins were filled with approximately 15 g field-moist, fine-fraction soil and weighed. Soil-filled tins were placed in a drying oven set at 55 °C. Dry

Table 1 Description of field sites

Biome	*Sites*	*Latitude, longitude*	*Mean[a] annual precip. (mm)*	*Max., min. air temp. (°C)*	*Mean[a] air temp. (°C)*	*Soil description*	*% Carbon by mass[a], top 0–10 cm (mean ± s.d.)*	*% Moisture by mass, top 0–10 cm (mean ± s.d.)*	*Incubation dates (m/d/y)*	*Weather during 7-day incubation*		
										Total precip. (mm)	*Max., min. air temp. (°C)*	*Mean air temp. (°C)*
Redwood forest	Jackson Demonstration State Forest's Caspar Creek watersheds: KJE[b], M	39° 22' N, 123° 42' W; elev. 146–216 m	1103	37.8, −3.9	10.8	Ultic Hapludalfs & Typic Haplohumults from weathered sandstone and shale. Well-drained. pH 6.07–6.25 (Dahlgren, 1998)	8.22 ± 0.17 control 7.15 ± 0.23 clearcut	28.1 ± 3.3 control 28.2 ± 4.1 clearcut	11/8/14–11/15/14	14.2	17.0, 8.4	13.0
Oak woodland	UC Hopland Research & Extension Center (HREC) watersheds: Foster (2 sites), Foster Biological (2 sites)[c, d]	39° 01' N, 123° 05' W; elev. 667 m	1016	33.3, 12.0	14.95	Typic Haploxeralfs and Ultic Argixerolls from weathered graywacke, shale, siltstone or sandstone. Well-drained. Loam texture (40% sand, 35% silt, 25% clay) (Dahlgren *et al.*, 2003). pH 6.19–7.16	3.29 ± 0.05 control 2.05 ± 0.06 burn only 4.71 ± 0.50 burn and graze 4.51 ± 0.09 graze only	22.3 ± 6.6 control 13.5 ± 3.3 burn only	No incubation	NA	NA	NA
Chaparral	HREC watersheds: James III (2 sites)[b]	39° 00' N, 123° 05' W	1016	33.3, 12.0	14.95	Typic Argixerollsfrom sandstone, shale and metasedimentary rock (Narvaez, 2007)	0.98 ± 0.11 control 1.58 ± 0.02 burn	12.7 ± 3.9 control 12.9 ± 5.5 burn	11/9/14–11/16/14	22.1	20.0, 7.8	13.9
Desert	Sweeney Granite Mountains Desert Research Center: under shrub, in interstitial spaces	34° 47' N, 115° 39' W; elev. 1252 m	292	33.0, −1.0	17.0	Granite-based, weakly developed, coarse. pH 7.0	0.90 ± 0.12 under shrub 0.34 ± 0.00 interstitial	6.6 ± 9.5 under shrub 1.8 ± 1.0 interstitial	2/2/14–2/9/14	0	13.3, 3.9	8.3

[a]Mean annual precipitation and air temperature data are long-term normals (1981–2010) from NOAA climate stations in Fort Bragg, Ukiah and Mitchell Caverns, CA, USA. Carbon data from UC Davis Stable Isotope Facility analysis of bulk N and C isotope data from dry soil with Micro Cube elemental analyzer interfaced to a PDZ Europa 20-20 Isotope-Ratio Mass Spectrometer. [b]Clearcut disturbances occurred in the KJE redwood site in 1989. [c]Fire disturbances occurred in one of the Foster and Foster Biological oak woodland sites in 2003, as well as in one of the chaparral sites in 2004. [d]Prescribed sheep grazing occurred at both Foster oak woodland sites.

weights were recorded after 48 h or when soil was completely dry. Moisture was calculated as water weight of the total sample and was used to transform field-moist weights in future analyses into soil dry weights.

KCl extractable soil nitrate

Soil inorganic N was extracted in-field with a 2 M potassium chloride (KCl) solution within 4 h of sample collection. The method was adapted from Keeney and Nelson to the field-setting (Keeney and Nelson, 1982). HDPE Nalgene containers were triple-rinsed daily in high-purity water for three days prior to usage. The 2 M KCl solution was prepared with high-grade KCl and high-purity water in a clean Nalgene container sealed with a twist-on cap and parafilm to prevent leakage during travel. A 50 ml volume of 2 M KCl and approximately 10 g field-moist soil were both measured into 60 ml-capacity sterile polypropylene specimen containers, which were then tightly sealed with twist-on caps. Samples were shaken vigorously for 5 min, left to settle upright for 5 min, shaken again for 2 min, and then left to settle upright for 2 h. The supernatant was filtered through funnels lined with ashless Whatman No.1 paper filters, which had been pre-washed with the 2 M KCl solution. The filtrate was collected in clean 60 ml-capacity HDPE Nalgene containers, which were immediately stored in a freezer or kept on constant ice in a cooler for later quantitative analyses in our UC Davis lab.

Colorimetric methods were used to quantify KCl extractable soil NO_3^-. A Griess reagent was added to samples in semi-micro cuvettes, with a 1:1 ratio in most cases, adjusted for greater sensitivity with lower concentrations (Doane and Horwáth, 2003). Vanadium(III) chloride reagent produced a red color indicating NO_3^-, which was measured after 8 h at 540 nm in a spectrophotometer (Miranda *et al.*, 2001; Doane and Horwáth, 2003). NO_3^- was calculated based on a standard curve created with stock potassium nitrate solution. A minimum 1 μM NO_3^- in the KCl extract was required for isotope analyses.

$^{15}N/^{14}N$ and $^{18}O/^{16}O$ analysis

Natural abundance of $^{15}N/^{14}N$ and $^{18}O/^{16}O$ in soil NO_3^- extracts were analyzed via a ThermoFinnigan PreCon-GasBench interfacing a Delta V Plus isotope-ratio mass spectrometer (Rock and Ellert, 2007) at UC Davis' Stable Isotope Facility. Samples were stored at −20 °C and thawed and mixed thoroughly before analysis. The denitrifier method was used to convert NO_3^- (and any trace NO_2^-) to N_2O, which was purged from vials, passed through an Ascarite CO_2 scrubber, and concentrated in two subsequent liquid N_2 cryo-traps (Sigman *et al.*, 2001; Casciotti *et al.*, 2002). A He stream (25 ml min^{-1}) carried the gas sample through this trace gas concentration system and then through an Agilent GS-Q capillary column (1.0 ml min^{-1}, 30 m × 0.32 mm, 40 °C).

International NO_3^- isotope standards USGS 32, USGS 34, and USGS 35 (National Institute of Standards and Technology, Gaithersburg, MD, USA) were used to calibrate the instrument, in addition to batch standards to account for drift. International reference standards were used to calculate isotope composition $-N_2$ in air for $\delta^{15}N$ and Vienna Standard Mean Oceanic Water (VSMOW) for $\delta^{18}O$.

NO_3^- isotope composition was corrected for the small KCl blank as follows:

$$\delta X_{sample} = \frac{\delta X_{total} - \delta X_{KCl\ blank} \times f_{KCl\ blank}}{f_{sample}}$$

where X = N or O isotopes of nitrate, and f = fraction nitrate of total nitrate.

Soil DNA extractions

DNA was extracted from ~0.25 g fine-earth fraction (<2 mm) soil—corrected for moisture—into 100 μl aliquots using Mo-Bio PowerSoil DNA Isolation Kit (Mo Bio Laboratories, Carlsbad, CA, USA) following manufacturer instructions. To verify a successful extraction and to quantify double-stranded DNA (dsDNA), the Qubit fluorometer (Thermo Fisher Scientific, Carlsbad, CA, USA) assay was used with Quant-iT dsDNA Broad Range reagent and buffer. DNA extracts yielding detectable dsDNA were then stored at −20 °C according to the Mo-Bio PowerSoil DNA Isolation Kit.

qPCR to determine functional gene abundances

Real-time qPCRs were used to detect and quantify specific functional genes of interest: nitrite reductase genes *nirK* and *nirS* ($NO_2^- \rightarrow NO$, the denitrification step with most isotopic fractionation), and bacterial 16S rRNA (the gene encoding for a highly conserved region in prokaryotic organisms, estimating total bacterial population). The genes of interest were amplified with specific target primers and thermal conditions and observed using fluorescent dye. The primers used for *nirS* were nirSCd3aFm and nirSR3cdm (Throback *et al.*, 2004). The *nirK* primers were nirK876 and nirK1040 (Henry *et al.*, 2004). The 16S rRNA primers were 341F and 534R (Lopez-Gutierrez *et al.*, 2004). See Supplementary Materials for full primer sequence descriptions and thermal conditions.

Standards were pre-made with serial dilutions of target DNA cloned into a plasmid (Scow Laboratory, UC Davis, Davis, CA, USA). Each total reaction had 5 μl template DNA (various dilutions for optimal detection), 12.5 μl SYBR GreenER qPCR SuperMix (Invitrogen, stored at 4 °C), 0.5 μM forward and reverse primers, and nanopure autoclaved deionized water for a 25 μl total volume. All standards, environmental samples and controls were run in

triplicate in Optical 96-Well Fast Thermal Cycling Plates via Applied Biosystems 7300 Real-Time PCR System.

Gene copies/g dry soil = [(mean quantity target gene detected)/5 µl sample] × (dilution factor × 100 µl original aliquot)/g dry soil. Mean quantity target gene detected = 10^((*n* − *b*)/*m*), where *n* = the number of cycles required for the fluorescent signal to exceed the background level, and *m* and *b* are the slope and y-intercept of the standard curve. A slope of −3.5 ± 0.4 is acceptable with $R^2 > 0.99$.

Statistics and analysis

Means and standard errors of the natural logarithm of KCl extractable soil nitrate (NO_3^-), $\delta^{15}N$ of NO_3^-, $\delta^{18}O$ of NO_3^-, and *nirS* abundance were regressed for sites for which > three parameter sets of values were detected. Using the natural logarithm of NO_3^- allowed us to perform linear regressions. Data distributions were normal or near-normal for all parameters based on normal quantile plots. Least-squares regression analyses determined the linear fit of all scatterplots, and we reported *R*-squared and *P*-values of regression slopes. *P*-values less than 0.05 were considered significant; at a 95% confidence level we reject the null hypothesis that there is no effect among variables.

We were unable to assemble full data sets of all target parameters for each site, owing to detection limits on NO_3^- concentrations (KCl sample extracts with <1 µM NO_3^- prevented samples from being analyzed for stable N and O isotopes). We focused results on sample sites wherein at least three samples were collected with detectable ensembles of NO_3^- concentrations, and abundance of isotopes and *nirS*. In the case of oak-woodland sites, criteria of triplicate *nirS* abundance data from at least three samples were not met; however, we were able to measure oak woodland N and O isotopes. Hence we include these data in analysis of isotopes but not the fully coupled analysis of isotopes, gene abundances and NO_3^- concentrations. Significant outliers detected via leverage and Cook's distance analyses were removed.

Stepwise regressions for $\delta^{15}N$- NO_3^- and *nirS* abundance were performed for incubation samples with the following data at a 95% confidence level: average field soil moisture for top 10 cm, average field %C for top 10 cm soil, mean air temperature, soil moisture in the incubation, *nirS* abundance, *nirK* abundance, 16S rRNA abundance, *nirS*/16S rRNA, *nirK*/16S rRNA, ln[NO_3^-], O and N isotopes from NO_3^-. These stepwise regressions were repeated for incubation samples from 7-day incubations which displayed decreased NO_3^- concentrations and had $\delta^{15}N > 0$, representing samples with denitrification as the dominant NO_3^- loss process that had occurred. Results from these analyses steered the focus of the figures and discussion toward select relationships.

Results

Soil nitrate and isotope composition patterns

Soil NO_3^- concentrations differed substantially across sites, generally tracking changes in MAP and soil C concentrations among terrestrial biomes (Table 1, Figure 2). NO_3^- concentrations were lowest in the mesic redwood site, and increased into the drier ecosystems, with a peak concentration observed for the desert sites, particularly in samples collected beneath creosote vegetation (Figure 2). The $\delta^{15}N$ of KCl extractable NO_3^- was negatively related to its concentration; highest mean $\delta^{15}N$-NO_3^- was observed for redwood sites (control 11.67 ± 1.09‰, clearcut 10.79 ± 0.53‰), intermediate values were apparent in the chaparral (1.56 ± 1.37‰), and lowest values were observed for the desert sites (under shrub 0.85 ± 0.32‰, interstitial −0.88 ± 2.53‰) (Figure 2). Highest mean $\delta^{18}O$-NO_3^- values were observed in redwood control (11.03 ± 2.19‰) and chaparral (11.61 ± 1.21‰), intermediate in redwood clearcut (4.22 ± 0.71‰), and lowest in desert sites (under shrub 0.47 ± 0.69‰, interstitial −1.28 ± 0.76‰) (Figure 2). $\delta^{15}N$-NO_3^- positively related with soil C ($R^2 = 0.22$, $P << 0.05$).

Linear regressions indicated several statistically significant relationships among soil NO_3^- isotopes and concentrations. Field surface $\delta^{15}N$-NO_3^- and $\delta^{18}O$-NO_3^- were positively correlated, with a linear slope for all surface soil isotope values at 0.55 ($R^2 = 0.25$, $P = 0.0002$) (Figure 3). If excluding sites without sufficient corresponding *nirS* data (that is, no oak woodland), the slope lowered to 0.47 ($R^2 = 0.17$, $P = 0.005$). A significant, negative relationship was observed between soil NO_3^- concentrations and $\delta^{15}N$-NO_3^- across all sites examined ($R^2 = 0.19$, $P = 0.003$) (Figure 5).

A positive relationship between $\delta^{15}N$-NO_3^- and $\delta^{18}O$-NO_3^- was observed in the *in-situ* 7-day surface soil (10 cm) incubations at the redwood and chaparral sites (Figure 6). In these ecosystems, decreased NO_3^- concentrations were strongly related to an increase in $\delta^{15}N$-NO_3^- ($R^2 = 0.50$, $P = 0.01$, $n = 11$). In contrast, there was no clear linear relationship for N and O isotopes from desert incubations, despite declines in NO_3^- concentrations during the incubation experiments ($R^2 = 0.00$, $n = 15$; Figure 6).

nirS gene abundance patterns

Mean *nirS* abundance averaged ~10^7 copies g^{-1} dry soil across sites. Abundances were highest in the redwood site ($7.43 \times 10^7 \pm 1.22 \times 10^7$ copies g^{-1} in redwood control, $6.04 \times 10^7 \pm 1.32 \times 10^7$ copies g^{-1} in redwood clearcut) and lowest in the desert sites ($2.64 \times 10^6 \pm 1.22$ x10^5 copies g^{-1} under creosote bush, $9.66 \times 10^6 \pm 2.65 \times 10^6$ copies g^{-1} in the interstitial spaces; Figure 2). *nirS* abundance positively correlated with soil C ($R^2 = 0.51$, $P << 0.05$).

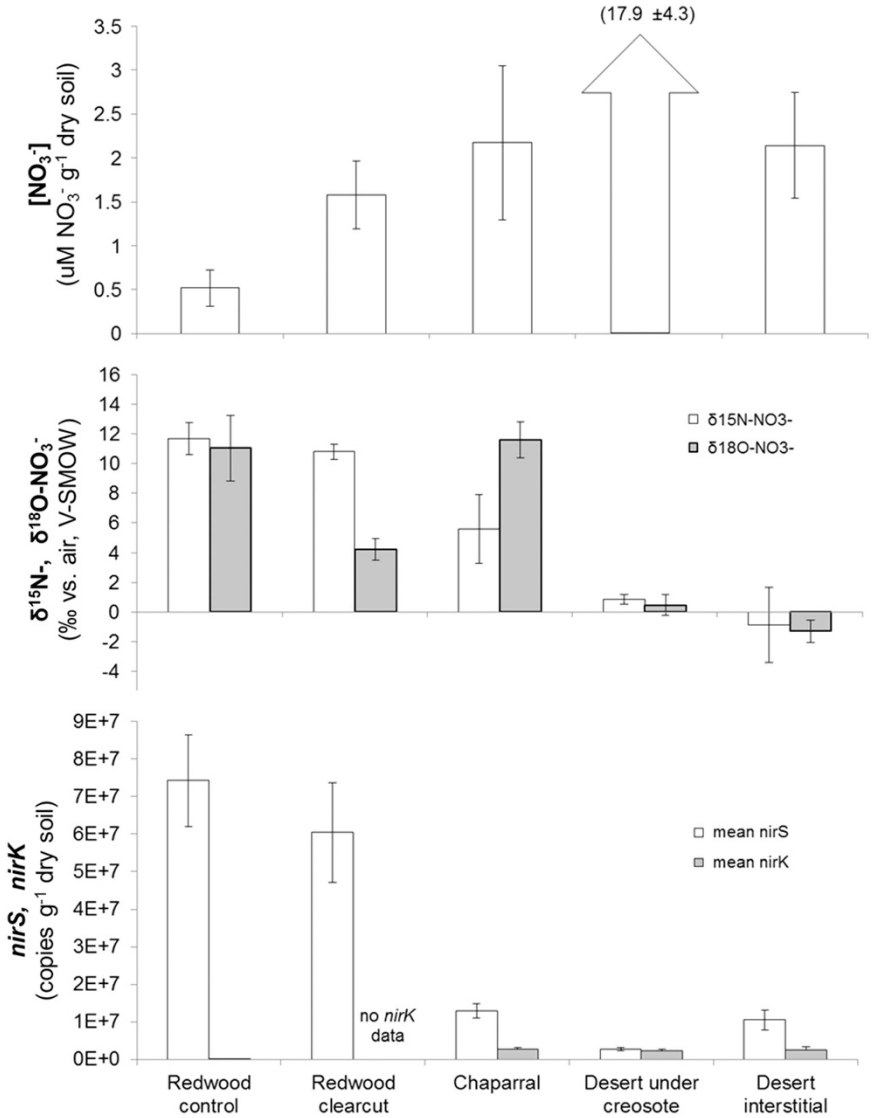

Figure 2 Surface soil NO_3^-, δ^{15}N-NO_3^- and *nirS* across sites. Includes sites with full study data set (N and O isotopes, extractable NO_3^-, *nirS*). $n = 9$ (redwood control, 13 for NO_3^-), 3 (redwood clearcut), 11 (chaparral, 14 for NO_3^-), 15 (desert under creosote), and 14 (desert interstitial). Bars are standard error.

Relationships between isotope composition and nirS

nirS and δ^{15}N-NO_3^- were significantly positively related across all sites ($R^2 = 0.35$, $P = 0.00002$) (Figures 2 and 4), and both parameters exhibited significant negative relationships with NO_3^- concentrations (*nirS* $R^2 = 0.20$, $P = 0.002$; δ^{15}N-NO_3^- $R^2 = 0.19$, $P = 0.003$; Figures 2 and 5). Although the distribution of field *nirS* data appears bi-modal (Figure 2), the Breusch-Pagan Test revealed homoscedasticity of the error terms ($P > 0.05$) for a linear regression model of ln[NO_3^-] vs *nirS* (Figure 4). *nirS* abundances and δ^{15}N-NO_3^- were highest in the undisturbed redwood site, which corresponded with the lowest soil extractable NO_3^- concentrations (Figure 2). The desert soils under the creosote vegetation exhibited the highest soil extractable NO_3^- concentrations, lowest *nirS* abundance and δ^{15}N-NO_3^- near 0‰ (Figure 2).

Positive denitrifier gene-isotope relationships were likewise observed in the 7-day incubation experiments conducted in the redwood and chaparral sites. The decrease in NO_3^- was associated with both an increase in δ^{15}N-$NO_3^- > 0$ ($n = 11$) and increase in *nirS* ($R^2 = 0.15$, $P = 0.24$) in these ecosystems. Furthermore, *nirS*/16S rRNA exhibited a significant positive relationship with δ^{15}N-NO_3^- ($R^2 = 0.70$, $P = 0.001$; Figure 7) in the short-term incubation experiments. From stepwise multiple regressions of desert incubations with NO_3^- loss and positive N isotopes, δ^{15}N-NO_3^- responded negatively to ln[NO_3^-], positively to *nirS* abundance, negatively to *nirS*/16S rRNA and slightly negatively to δ^{18}O-NO_3^- (multiple $R = 0.86$, standard error s.e. = 7.4, $n = 15$, significance $F < 0.05$). For stepwise regressions of corresponding redwood and chaparral incubations, δ^{15}N-NO_3^- responded negatively to ln

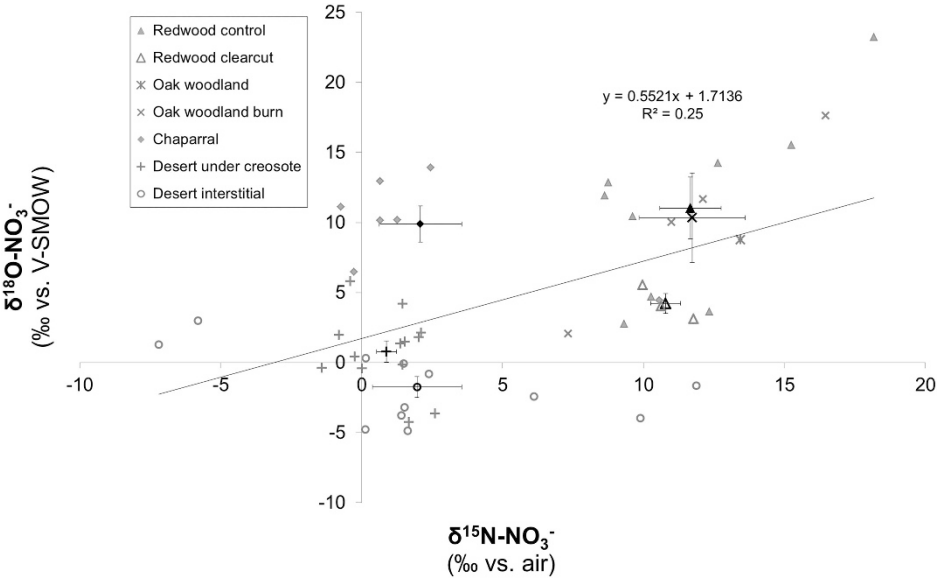

Figure 3 δ^{18}O-NO_3^- vs δ^{15}N-NO_3^-. Bold symbols are mean values per site. Bars are standard error. Linear regression for field surface soil datapoints is $y = 0.55x + 1.71$ ($R^2 = 0.25$, $P = 0.00026$, $n = 49$). Outliers identified via leverage analyses were removed. If excluding sites without sufficient corresponding *nirS* data (that is, no oak woodland), $y = 0.47x + 1.86$ ($R^2 = 0.17$, $P = 0.005$, $n = 44$).

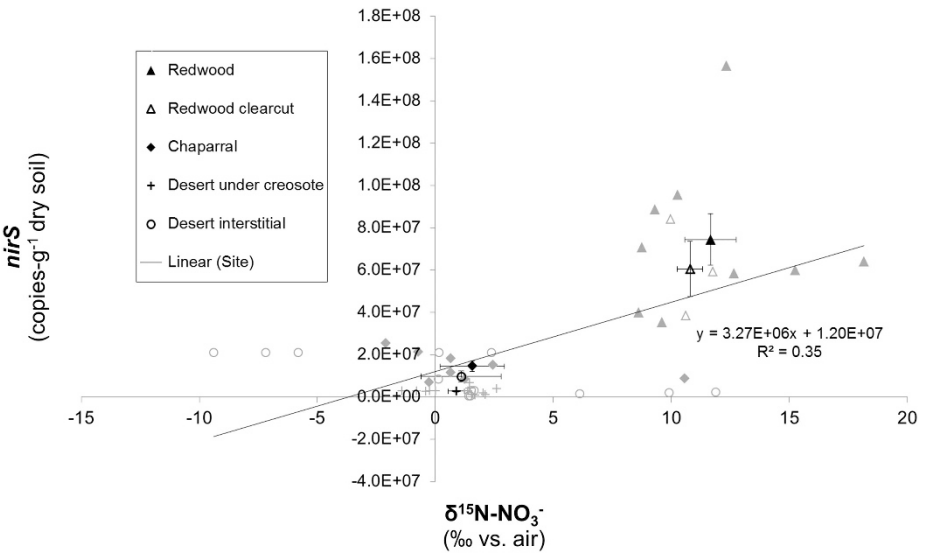

Figure 4 *nirS* vs δ^{15}N-NO_3^-. Bold symbols are mean values per site. Bars are standard error. Linear regression for all datapoints is $y = 3.27E\text{^}6x + 1.20E\text{^}7$ ($R^2 = 0.35$, $P = 0.00002$).

[NO_3^-], not significantly with *nirS* abundance, and positively to δ^{18}O-NO_3^- (multiple $R = 0.95$, s.e. = 2.01, $n = 11$, significance $F << 0.05$).

$$\text{Desert } \delta^{15}\text{N} - \text{NO}_3{}^- = 20.54 - 5.09 * \ln[\text{NO}_3{}^-] + \left(5.92 \times 10^{-6}\right) * nirS - 8762.48 * (nirS/16S) - 1.38 * \left(\delta^{18}\text{O} - \text{NO}_3{}^-\right)$$

$$\text{Redwood and Chaparral } \delta^{15}\text{N} - \text{NO}_3{}^- = -1.94 - 2.84 * \ln[\text{NO}_3{}^-] + 0.68 * \delta^{18}O - \text{NO}_3{}^-$$

Other environmental and microbial variables included at the start (temperature, carbon, moisture, *nirK*, *nirK*/16S) did not have a significant relationship with δ^{15}N-NO_3^- by the end of the stepwise regressions. These results were from stepwise regressions set at 95% confidence. Differences in linear response to δ^{18}O-NO_3^- alone are shown in Figure 6. Denitrifier linear responses to δ^{15}N-NO_3^- are shown in Figure 7.

Discussion

Our findings support the first hypothesis—that variations in terrestrial δ^{15}N are controlled primarily

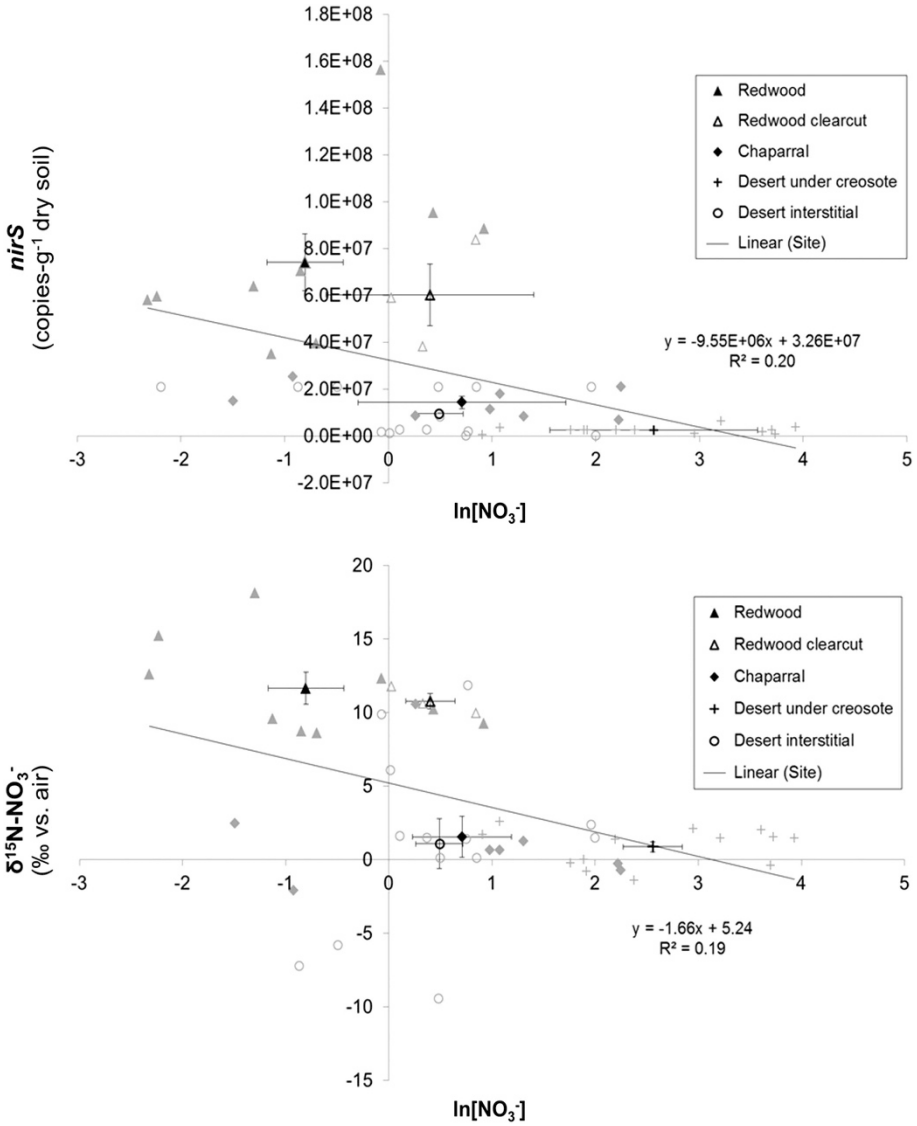

Figure 5 *nirS* (top) and δ^{15}N-NO_3^- (bottom) vs ln[NO_3^-]. Soil extractable nitrate concentration prior to logarithmic transformation was in units of μM NO_3^- g^{-1} dry soil. Bold symbols are mean values per site. Bars are standard error. Linear regressions for all datapoints: *nirS* $y = -9.55E+06x + 3.28E+07$ ($R^2 = 0.20$, $P = 0.002$); δ^{15}N-NO_3^- $y = -1.66x + 5.24$ ($R^2 = 0.19$, $P = 0.003$).

by biogenic gaseous emissions of N (Houlton and Bai, 2009), principally isotopic discrimination via denitrifying organisms' enzyme-systems (Mariotti *et al*., 1981). This result agrees with the elevated δ^{15}N of N inputs compared to that of N leaching losses in our sites (Mnich and Houlton, 2015), and furthermore is consistent with global scale imbalance between input δ^{15}N and the residual N of the terrestrial biosphere (Houlton and Bai, 2009; Vitousek *et al*., 2013). In addition, the negative relationships between ecosystem NO_3^- availability and δ^{15}N/*nirS* support the second hypothesis—that microbial denitrification can consume NO_3^- to low levels in terrestrial ecosystems, even in temperate environments where N limitation is widespread (LeBauer and Treseder, 2008). The incubation portion of our study further identifies the capacity for denitrifiers to rapidly consume NO_3^- to low levels within a given site. Overall, these findings are at odds with general formulations of denitrification in contemporary ecosystem models (for example, CENTURY, Davidson and Seitzinger, 2006), which simulate an increase in this process with increasing soil NO_3^- supplies. Rather, the evidence points to direct control of denitrifiers over soil NO_3^- availability patterns, which, over time, help to explain the persistence of N limitation observed for grassland to forest ecosystems (Vitousek and Howarth, 1991, LeBauer and Treseder, 2008).

One possible explanation for the denitrifier-driven effect on soil NO_3^- is that plants in these sites rely on NH_4^+ and/or direct uptake of amino acids to meet their N demands, thereby allowing denitrifiers to consume NO_3^- to relatively low levels. This interpretation is consistent with elevated δ^{15}N and δ^{18}O where NO_3^- is low vs high; plant reliance on NO_3^-

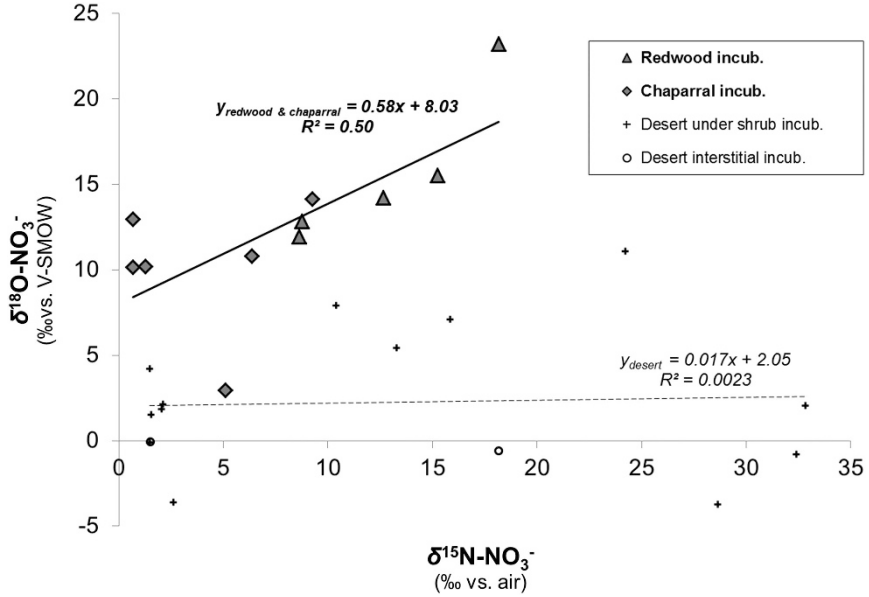

Figure 6 δ^{18}O-NO_3^- vs δ^{15}N-NO_3^- incubations. Includes initial and final subsamples from 7-day incubations for which [NO_3^-] decreased and δ^{15}N-NO_3^- > 0. Linear regression for redwood and chaparral incubations is $y = 0.58x + 8.03$ ($R^2 = 0.50$, $P = 0.01$, $n = 11$). Linear regression for desert incubations is $y = 0.017x + 2.05$ ($R^2 = 0.00$, $n = 15$).

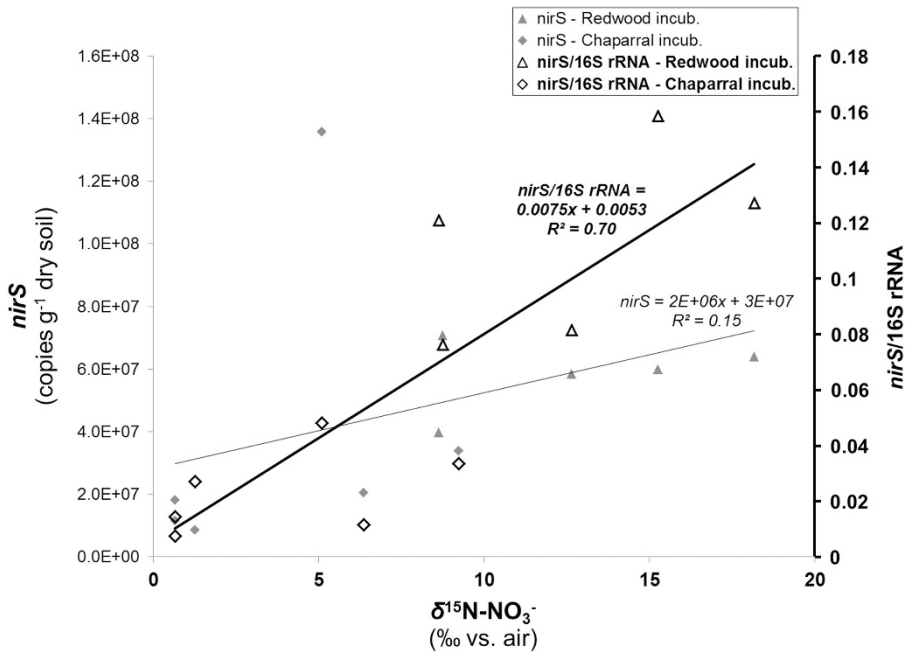

Figure 7 Denitrifiers vs δ^{15}N-NO_3^- in redwood and chaparral incubations. Data include any initial and final subsamples from redwood and chaparral 7-day *in-situ* incubations for which [NO_3^-] decreased and δ^{15}N-NO_3^- > 0 ($n = 11$). Linear regression for *nirS*/16S rRNA is $y = 0.0075x + 0.0053$ ($R^2 = 0.70$, $P = 0.001$). Regression for *nirS* is $y = 2.0 \times 10^6 x + 3 \times 10^7$ ($R^2 = 0.15$, $P = 0.24$).

would not impart such significant isotope effects. Moreover, denitrifiers may directly out-compete plants and other microbes for NO_3^- in moist and C-rich environments, perhaps taking advantage of strong redox potential gradients across soil aggregates in the forest and savanna sites (Sexstone *et al.*, 1985; Ebrahimi and Or, 2016). Indeed, the significant positive correlations between *nirS* ($R^2 = 0.51$, $P << 0.05$) and δ^{15}N-NO_3^- ($R^2 = 0.22$, $P << 0.05$) vs soil C concentrations across our terrestrial sites point to the likelihood of this mechanism. It is worthwhile to note that aggregate pore sizes can influence anoxic zones and greenhouse gas diffusion/emissions, even in unsaturated and variable field conditions (Ebrahimi and Or, 2016), although we did not study aggregates closely in these sites.

Temperature is another environmental factor to consider, as our sites exhibited a gradient in mean air temperatures (Table 1). Temperature increases have been shown theoretically and empirically to influence the kinetics of denitrification-driven isotopic fractionation (Maggi and Riley, 2015). The affinity for biological NO_3^- fractionation increases with temperature, and Maggi and Riley, 2015 accurately modeled this nonlinear phenomenon at a range of temperatures (20-35 °C), even with heterogeneous soils. While air temperature was not as closely related to isotopic data as other variables were in our study, it is not outside the realm of possibility that soil temperatures, which were not measured, influenced the patterns observed.

Furthermore, other N transformation processes could play a role in influencing available NO_3^- pools and potentially $\delta^{15}N$, including: nitrification, heterotrophic immobilization and potentially dissimilatory NO_3^- reduction to NH_4^+ (DNRA). Nitrification is a fractionating process that acts to lower the $\delta^{15}N$ of NO_3^- vs that of NH_4^+ substrates, whereas both heterotrophic microbial assimilation and DNRA would be expected to impart an isotope effect on NO_3^- that resembles that of denitrification.

However, additional evidence for principal denitrifier controls over NO_3^- concentrations is apparent in dual-isotope relationships in our study (Figure 3). Specifically, a positive relationship between $\delta^{18}O$ and $\delta^{15}N$ with a slope near 0.6 is diagnostic of terrestrial denitrification, because denitrifying bacteria preferentially convert both light isotopes in NO_3^- to gaseous products (Lehmann *et al.*, 2003). Heterotrophic NO_3^- immobilization also fractionates against O and N isotopes in NO_3^-; though at a much higher slope, typically between 1.0 and 2.0 (Granger *et al.*, 2010). Our observed 0.55 slope for field sites ($R^2 = 0.25$, $P = 0.00026$) is therefore consistent with the imprint of terrestrial denitrifiers on soil NO_3^- consumption (Figure 3), as seen in previous work in tropical and temperate forest soils (Houlton *et al.*, 2006; Fang *et al.*, 2015). We cannot specifically address why the slopes differ across studies, but past work on marine bacteria cultures indicates that chemolithotrophs fractionate a slope closer to 0.5, whereas heterotrophic denitrifiers appear to fractionate O and N isotopes at a higher slope (Frey *et al.*, 2014). Differences between microbial effects on O and N isotope relationships generally reflect differences in kinetic rate transfers of isotopes from substrates to products and O exchange reactions with water and air. Indeed, variations in the isotopic composition of O source for NO_3^- could explain the $\delta^{18}O$-NO_3^- differences observed across our ecosystem sites (for example, redwood control vs clearcut in Figure 2).

Moreover, the spatial patterns observed across sites are similarly observed in our short-term incubation experiments (that is, 7 days), thus pointing to the importance of microbial denitrifiers in driving soil NO_3^- availability patterns in both space and time. Aerobic nitrification and even atmospheric deposition may have slightly diminishing effects on N and O isotopes of NO_3^- in an open system; and so the relationship between N and O isotopes of NO_3^- in anaerobic incubations is of particular interest. Indeed, $\delta^{15}N$ and $\delta^{18}O$ of NO_3^- in the soil incubation experiments reveal a slope that matches expectations for marine and freshwater denitrifiers (Lehmann *et al.*, 2003; Granger *et al.*, 2008) and observations for other terrestrial ecosystems (Houlton *et al.*, 2006; Fang *et al.*, 2015), similar to the spatial relationships observed for all samples across sites (that is, ~ 0.6) (Figure 6). Not only did we observe a positive relationship between *nirS* and $\delta^{15}N$-NO_3^- mirroring the cross-system results; but there was a significant positive correlation between *nirS*/16S rRNA and $\delta^{15}N$-NO_3^- in our soil incubation experiments as well ($R^2 = 0.70$, $P = 0.001$) (Figure 7). This demonstrates that the microbial community composition was rapidly enriched in organisms with denitrifying genes, which explains the increase in $\delta^{15}N$ and $\delta^{18}O$ that accompanied declining NO_3^- concentrations. Such community streamlining has been observed in aquatic environments (Jayakumar *et al.*, 2009), but, to our knowledge, these are the first observations for terrestrial soil-systems. In sum, these findings support our conclusion that denitrifiers played a major role in determining NO_3^- pool sizes across sites, with isotopic and molecular evidence revealing complementary patterns across scales, from induced short-term consumption events to the determination of cross-site patterns among biomes.

Importantly, the inverse relationships between $\delta^{15}N$-NO_3^- and soil NO_3^- concentration is observed across sites (Figures 2 and 5); however, the calculated isotope effects were much lower than those observed in pure cultures of denitrifying bacteria. The isotope effect of denitrification ranges from 0‰ to ~ − 33‰ (Högberg, 1997), with an average of approximately -20 ± 1.0‰ observed for laboratory studies (Delwiche and Steyn, 1970; Granger *et al.*, 2008; Houlton and Bai, 2009). The magnitude of the isotope effect can be lower in the field, particularly in environments where non-homogenous interactions allow for locally complete NO_3^- consumption, as in a 'closed system' Rayleigh model (Brandes and Devol, 2002; Houlton *et al.*, 2006). In this case, NO_3^- can be completely consumed in micro-environments leaving little or no residual NO_3^- to express denitrification's isotope effect (Houlton *et al.*, 2006). Furthermore, non-fractionating sinks such as plant uptake and microbial assimilation can consume NO_3^- without altering $^{15}N/^{14}N$. In our sites the relationship between $\delta^{15}N$ and $\ln[NO_3^-]$ suggests an integrated isotope effect—a net isotope effect reflecting all NO_3^- sources and sinks—that varies from -2.12 in the redwood site to 1.92 in the desert interstitial site, with an overall effect across sites of − 1.66.

One exception to the inverse relationship between $\delta^{15}N$-NO_3^- and soil NO_3^- is evident in the desert soil, particularly beneath vegetation canopies. The soil

devoid of vegetation had notably lower [NO_3^-] than those collected under *L.tridentata* 'islands of fertility'; and yet the interstitial sites had the same, if not lower, δ^{15}N-NO_3^- as the vegetated ones (Figure 2). The weakly positive relationships in interstitial spaces suggest that nitrification, ammonia volatilization or other abiotic processes could be responsible for gaseous N production in such arid environments (McCalley and Sparks, 2009). It is possible that in arid and wind-prone desert ecosystems, uptake of NO_3^- by heterotrophic microbes and plants could mask any denitrification-driven enrichment of heavy N and O isotopes. Any substantial non-fractionating sinks for NO_3^- could greatly reduce the isotope effect of denitrifiers. We cannot rule out the role of episodically driven effects on denitrification in the desert, where precipitation occurs over very short, high-intensity events.

The field portion of our study provides useful, integrated snapshots of O and N isotopes of NO_3^- in a variety of field settings—taking into account the collective effects of ecosystem N cycling. The incubation experiments help to isolate the field-based evidence for denitrifier-driven controls over soil NO_3^-, albeit under optimal conditions of low O_2 availability. Future work in such dynamic systems could benefit from long-term, daily field studies coupled with field-sensors of soil moisture, pH, temperature and redox.

Implications for linking microbial gene abundance to ecosystem functioning

Our results have implications for understanding linkages among microbial functional gene abundances and ecosystem pattern and process. As modern genetic techniques have tremendously increased, questions over the utility of microbial gene abundance measures have become paramount, representing a key area of active research in the microbial ecology and ecosystem biogeochemistry. Our finding of a positive correlation between gene abundance and isotope composition provides a new, integrative tool for connecting DNA to variations in ecosystem NO_3^- pools and natural isotope composition; it reveals a link between genes encoding for a given enzyme (for example, *nirS*) and its role in a key ecosystem process (for example, denitrification) across biomes. We suspect that such a 'gene abundance to isotope' relationship is likely best observed in wet seasons or generally moist sites, owing to denitrifiers' ability to thrive in high moisture and anaerobic soil environments where C is abundant (Dawson and Murphy, 1972; Burgin *et al.*, 2010; Szukics *et al.*, 2010; Groffman 2012).

Previous studies on relationships between *nirS/K* and terrestrial denitrification rates have been mixed, which could be explained by mismatches in the scale of measurements or artifacts of disturbance (Wallenstein *et al.*, 2006). Structure and abundance of microbial communities bearing *nirS* appear less sensitive to long-term fertilizations than those with *nirK* (Chen *et al.*, 2010), and actual transcription of *nirS* is less sensitive to changes in pH than *nirK* (Liu *et al.*, 2014). Thus, our focus on *nirS* likely minimized the chances of localized factors from obscuring relationships between community structure, gene abundance and actual gene expression.

Terrestrial denitrification has remained a poorly understood aspect of N cycling research (Davidson and Seitzinger, 2006). Our results demonstrate a significant link between *nirS* and natural isotope abundance, over scales ranging from short-term soil incubation experiments to the factors structuring longer-term soil NO_3^- pools across forest to desert ecosystems. Kinetic isotopic discrimination is the result of denitrifying organisms' enzymatic preferences for light isotopes in NO_3^-. Thus, while gene abundance data alone do not represent the diversity or activity of soil microbial communities, the relationships between *nirS* and heavy isotope enrichment point to tight connections between denitrifier gene abundances and microbial enzyme activity across our sites. Where N availability is highest in the desert biome, the imprint of denitrification appears weakest; where N availability was lowest, coupled molecular and isotopic data point to substantial NO_3^- consumption by denitrifying bacteria. These findings suggest that models of denitrification should be re-formulated to include a more direct influence of denitrifiers in determining terrestrial N availability.

Conflict of Interest

The authors declare no conflict of interest.

Acknowledgements

This project was supported by the National Science Foundation (Award #1150246, CAREER grant to Dr Benjamin Houlton). We thank Meagan Mnich for her collaboration on the project, research assistants John Baum, Hanna Morris, Angie Munguia, Caprice Lee, Vincent Ho and the Stable Isotope Facility at UC Davis. We thank Dr Kate Scow and Dr Randy Dahlgren for sharing equipment and feedback on microbial and nutrient data.

References

Attard E, Recous S, Chabbi A, De Berranger C, Guillaumaud N, Labreuche J *et al.* (2011). Soil environmental conditions rather than denitrifier abundance and diversity drive potential denitrification after changes in land uses. *Glob Chang Biol* **17**: 1975–1989.

Bai E, Houlton BZ, Wang YP. (2012). Isotopic identification of nitrogen hotspots across natural terrestrial ecosystems. *Biogeosciences* **9**: 3287–3304.

Bardgett RD, Lovell RD, Hobbs PJ, Jarvis SC. (1999). Seasonal changes in soil microbial communities along a fertility gradient of temperate grasslands. *Soil Biol Biochem* **31**: 1021–1030.

Beckman JS, Koppenol WH. (1996). Nitric oxide, superoxide, and peroxynitrite: the good, the bad, and the ugly. *Am J Physiol-Cell Physiol* **40**: C1424.

Braker G, Fesefeldt A, Witzel KP. (1998). Development of PCR primer systems for amplification of nitrite reductase genes (nirK and nirS) to detect denitrifying bacteria in environmental samples. *Appl environ microbiol* **64**: 3769–3775.

Brandes JA, Devol AH. (2002). A global marine-fixed nitrogen isotopic budget: implications for Holocene nitrogen cycling. *Glob Biogeochem Cycles* **16**: 1120.

Burgin AJ, Groffman PM, Lewis DN. (2010). Factors regulating denitrification in a riparian wetland. *Soil Sci Am J* **74**: 1826–1833.

Calderon FJ, Jackson LE, Scow KM, Rolston DE. (2001). Short-term dynamics of nitrogen, microbial activity, and phospholipid fatty acids after tillage. *Soil Sci Soc Am J* **65**: 118–126.

Casciotti K, Sigman D, Hastings M, Bohlke J, Hilkert A. (2002). Measurement of the oxygen isotopic composition of nitrate in seawater and freshwater using the denitrifier method. *Anal Chem* **74**: 4905–4912.

Chen Z, Luo X, Hu R, Wu M, Wu J, Wei W. (2010). Impact of long-term fertilization on the composition of denitrifier communities based on nitrite reductase analyses in a paddy soil. *Microb Ecol* **60**: 850–861.

Ciais P, Sabine C, Bala G, Bopp L, Brovkin V, Canadell J *et al.* (2013). *Carbon and other biogeochemical cycles*. Climate change 2013: The Physical Science Basis Contribution of Working Group I to the Fifth Assessment Report of the Intergovernmental Panel on Climate Change. p. 1535.

Dahlgren R, Horwath W, Tate K, Camping T. (2003). Blue oak enhance soil quality in California oak woodlands. *California Agric* **57**: 42–47.

Dahlgren RA. (1998). *Effects of forest harvest on stream-water quality and nitrogen cycling in the Caspar Creek watershed*. USDA Forest Service Gen Tech Rep PSW-GTR-168.

Davidson E, Seitzinger S. (2006). The enigma of progress in denitrification research. *Ecol Appl* **16**: 2057–2063.

Dawson RN, Murphy KL. (1972). The temperature dependency of biological denitrification. *Wat Res* **6**: 71–83.

Delwiche CC, Steyn PL. (1970). Nitrogen isotope fractionation in soils and microbial reactions. *Environ Sci Technol* **4**: 929–935.

Doane TA, Horwáth WR. (2003). Spectrophotometric determination of nitrate with a single reagent. *Anal Lett* **36**: 2713–2722.

Ebrahimi A, Or D. (2016). Microbial community dynamics in soil aggregates shape biogeochemical gas fluxes from soil profiles–upscaling an aggregate biophysical model. *Glob change biol* **9**: 3141–3156.

Falkowski PG, Fenchel T, Delong EF. (2008). The microbial engines that drive Earth's biogeochemical cycles. *science* **320**: 1034–1039.

Fang Y, Koba K, Makabe A, Takahashi C, Zhu W, Hayashi T *et al.* (2015). Microbial denitrification dominates nitrate losses from forest ecosystems. *Proc Natl Acad Sci USA* **112**: 1470–1474.

Frey C, Hietanen S, Jürgens K, Labrenz M, Voss M. (2014). N and O isotope fractionation in nitrate during chemolithoautotrophic denitrification by Sulfurimonas gotlandica. *Environ sci technol* **48**: 13229–13237.

Frey SD, Knorr M, Parrent JL, Simpson RT. (2004). Chronic nitrogen enrichment affects the structure and function of the soil microbial community in temperate hardwood and pine forests. *Forest Ecol Manage* **196**: 159–171.

Graf DR, Jones CM, Hallin S. (2014). Intergenomic comparisons highlight modularity of the denitrification pathway and underpin the importance of community structure for N 2 O emissions. *PloS one* **9**: e114118.

Granger J, Sigman D, Rohde M, Maldonado M, Tortell P. (2010). N and O isotope effects during nitrate assimilation by unicellular prokaryotic and eukaryotic plankton cultures. *Geochim Cosmochim Acta* **74**: 1030–1040.

Granger J, Sigman DM, Lehmann MF, Tortell PD. (2008). Nitrogen and oxygen isotope fractionation during dissimilatory nitrate reduction by denitrifying bacteria. *Limnol Oceanogr* **53**: 2533.

Groffman P. (2012). Terrestrial denitrification: challenges and opportunities. *Ecol Processes* **1**: 11.

Helen D, Kim H, Tytgat B, Anne W. (2016). Highly diverse nirK genes comprise two major clades that harbour ammonium-producing denitrifiers. *BMC genom* **17**: 1.

Henry S, Baudoin E, Lopez-Gutierrez JC, Martin-Laurent F, Brauman A, Philippot L. (2004). Quantification of denitrifying bacteria in soils by nirK gene targeted real-time PCR. *J microbiol meth* **59**: 327–335.

Heylen K, Gevers D, Vanparys B, Wittebolle L, Geets J, Boon N *et al.* (2006). The incidence of nirS and nirK and their genetic heterogeneity in cultivated denitrifiers. *Environ microbiol* **8**: 2012–2021.

Hochstein LI, Tomlinson GA, Knowles R, Delwiche CC, Bryan BA, Payne WJ. (1988). The enzymes associated with denitrification; Denitrification: microbiology and ecology; Denitrification; Reduction of nitrogenous oxides by microorganisms. *Annu Rev Microbiol* **42**: 231–261.

Houlton B, Bai E. (2009). Imprint of denitrifying bacteria on the global terrestrial biosphere. *Proc Natl Acad Sci USA* **106**: 21713–21716.

Houlton B, Sigman D, Hedin L. (2006). Isotopic evidence for large gaseous nitrogen losses from tropical rainforests. *Proc Natl Acad Sci USA* **103**: 8745–8750.

Houlton BZ, Marklein AR, Bai E. (2015). Representation of nitrogen in climate change forecasts. *Nat Clim Change* **5**: 398–401.

Högberg P. (1997). Tansley Review No. 95 15N natural abundance in soil-plant systems. *New Phytol* **137**: 179–203.

Jackson L, Calderon F, Steenwerth K, Scow K, Rolston D. (2003). Responses of soil microbial processes and community structure to tillage events and implications for soil quality. *Geoderma* **114**: 305–317.

Jayakumar A, O'mullan G, Naqvi S, Ward B. (2009). Denitrifying bacterial community composition changes associated with stages of denitrification in oxygen minimum zones. *Microb ecol* **58**: 350–362.

Keeney D, Nelson D. (1982). *Nitrogen—inorganic forms*. Methods of soil analysis Part 2 Chemical and microbiological properties. American Society of Agronomy, Soil Science Society of America: Madison, WI, USA.

Knowles R. (1982). Denitrification. *Microbiol Rev* **46**: 43–70.

Kulkarni MV, Burgin AJ, Groffman PM, Yavitt JB. (2014). Direct flux and 15N tracer methods for measuring denitrification in forest soils. *Biogeochemistry* **117**: 359–373.

LeBauer DS, Treseder KK. (2008). Nitrogen limitation of net primary productivity in terrestrial ecosystems is globally distributed. *Ecol* **89**: 371–379.

Lehmann MF, Reichert P, Bernasconi SM, Barbieri A, McKenzie JA. (2003). Modelling nitrogen and oxygen isotope fractionation during denitrification in a lacustrine redox-transition zone. *Geochim Cosmochim Acta* **67**: 2529–2542.

Lennon EFE. (2015), Scaling terrestrial denitrificaiton at the nitrite reduction step: natural stable N isotopes and nirS genes in temperate biomes. MS thesis, University of California.

Levin SA. (1992). The problem of pattern and scale in ecology: the Robert H. MacArthur award lecture. *Ecology* **73**: 1943–1967.

Liu B, Frostegard A, Bakken LR. (2014). Impaired reduction of N2O to N2 in acid soils is due to a posttranscriptional interference with the expression of nosZ. *mBio* **5**: 01383–01314.

Lopez-Gutierrez JC, Henry S, Hallet S, Martin-Laurent F, Catroux G, Philippot L. (2004). Quantification of a novel group of nitrate-reducing bacteria in the environment by real-time PCR. *J microbiol meth* **57**: 399–407.

Maggi F, Riley WJ. (2015). The effect of temperature on the rate, affinity, and 15N fractionation of NO3—during biological denitrification in soils. *Biogeochemistry* **124**: 235–253.

Mariotti A, Germon J, Hubert P, Kaiser P, Letolle R, Tardieux A *et al.* (1981). Experimental determination of nitrogen kinetic isotope fractionation: some principles; illustration for the denitrification and nitrification processes. *Plant Soil* **62**: 413–430.

McCalley CK, Sparks JP. (2009). Abiotic gas formation drives nitrogen loss from a desert ecosystem. *Science* **326**: 837–840.

Miranda KM, Espey MG, Wink DA. (2001). A rapid, simple spectrophotometric method for simultaneous detection of nitrate and nitrite. *Nitric oxide* **5**: 62–71.

Mnich M, Houlton B. (2015). Evidence for a uniformly small isotope effect of nitrogen leaching loss: results from disturbed ecosystems in seasonally dry climates. *Oecologia* **181**: 323–333.

Narvaez N. (2007). Prescribed herbivory to reduce fuel load in California chaparral. Doctor of Philosophy, University of California: Davis, CA, USA.

Patra AK, Abbadie L, Clays-Josserand A, Degrange V, Grayston SJ, Loiseau P *et al.* (2005). Effects of grazing on microbial functional groups involved in soil N dynamics. *Ecol Monogr* **75**: 65–80.

Robinson D. (2001). δ 15 N as an integrator of the nitrogen cycle. *Trends Ecol Evolut* **16**: 153–162.

Rock L, Ellert BH. (2007). Nitrogen-15 and Oxygen-18 natural abundance of potassium chloride extractable soil nitrate using the denitrifier method. *Soil Sci Soc Am J* **71**: 355–361.

Sexstone A, Revsbech N, Parkin T, Tiedje J. (1985). Direct measurement of oxygen profiles and denitrification rates in soil aggregates. *Soil Sci Soc Am J* **49**: 645–651.

Sigman D, Casciotti K, Andreani M, Barford C, Galanter M, Bohlke J. (2001). A bacterial method for the nitrogen isotopic analysis of nitrate in seawater and freshwater. *Anal Chem* **73**: 4145–4153.

Smith MS, Tiedje JM. (1979). Phases of denitrification following oxygen depletion in soil. *Soil Biol Biochem* **11**: 261–267.

Szukics U, Abell GC, Hödl V, Mitter B, Sessitsch A, Hackl E *et al.* (2010). Nitrifiers and denitrifiers respond rapidly to changed moisture and increasing temperature in a pristine forest soil. *FEMS Microbiol Ecol* **72**: 395–406.

Throback IN, Enwall K, Jarvis A, Hallin S. (2004). Reassessing PCR primers targeting nirS, nirK and nosZ genes for community surveys of denitrifying bacteria with DGGE. *FEMS Microbiol Ecol* **49**: 401–417.

Torsvik V, Øvreås L. (2002). Microbial diversity and function in soil: from genes to ecosystems. *Curr opin microbiol* **5**: 240–245.

Vitousek PM, Howarth RW. (1991). Nitrogen limitation on land and sea: How can it occur? *Biogeochemistry* **13**: 87–115.

Vitousek PM, Menge DN, Reed SC, Cleveland CC. (2013). Biological nitrogen fixation: rates, patterns and ecological controls in terrestrial ecosystems. *Philos Trans R Soc London B: Biol Sci* **368**: 20130119.

Wallenstein MD, Myrold DD, Firestone M, Voytek M. (2006). Environmental controls on denitrifying communities and denitrification rates: insights from molecular methods. *Ecol appl* **16**: 2143–2152.

Williams E, Hutchinson G, Fehsenfeld F. (1992). NOx and N2O emissions from soil. *Glob Biogeochem Cycles* **6**: 351–388.

Zhu Q, Riley WJ. (2015). Improved modelling of soil nitrogen losses. *Nat Clim Change* **5**: 705–706.

Zumft WG. (1997). Cell biology and molecular basis of denitrification. *Microbiol mol biol rev* **61**: 533–616.

Supplementary Information accompanies this paper on *The ISME Journal* website (http://www.nature.com/ismej)